AIAA SciTech
5-9 January 2015, Kissimmee, Florida
AIAA Atmospheric Flight Mechanics Conference

Flight test results of Observer/Kalman Filter Identification of the Pegasus unmanned vehicle

Timothy Woodbury*, Frank Arthurs†, and John Valasek‡
Texas A&M University, College Station, TX, 77843-3141

Flight testing is the preferred means of obtaining accurate, locally linear, dynamic models of nonlinear aircraft dynamics. In this paper, decoupled longitudinal and lateral/directional linear dynamic models of an unmanned air vehicle are identified using the Observer/Kalman Filter Identification method. This method is a time-domain technique that identifies a discrete input-output mapping from known input and output data samples. The method is developed for flight testing, including details of instrumentation, measurements, and data post-processing techniques such as nonlinear estimation. Multiple flight tests were conducted, and experimental examples for longitudinal and lateral/directional dynamics are presented, including the model selection process. Fidelity of the identified linear models to the nonlinear plant is validated by comparing measured and model predicted outputs with measured inputs from flight test. Mean squared errors and the Theil information coefficient are used as accuracy metrics. Results presented in the paper demonstrate that the linear models reproduced from flight test results are acceptable representations of the nonlinear aircraft dynamics in the cruise configuration.

Nomenclature

α	angle-of-attack
β	sideslip angle
u	body 1-axis perturbed airspeed
p	aircraft roll rate
q	aircraft pitch rate
r	aircraft yaw rate
ϕ	aircraft roll angle
θ	aircraft pitch angle
ψ	aircraft heading angle
$\mathbf{x}$	vector x
T	discrete-time sample period
$\mathbf{x}_k$	value of discrete-time variable $\mathbf{x}$ at time Tk

Acronyms

ADC	Air Data Computer
APM	ArduPilot Mega
ERA	Eigensystem Realization Algorithm

*Graduate Research Assistant, Vehicle Systems & Control Laboratory, Department of Aerospace Engineering, Student Member AIAA, twoodbury@tamu.edu

†Graduate Research Assistant, Vehicle Systems & Control Laboratory, Department of Aerospace Engineering, Student Member AIAA, arthursf@neo.tamu.edu

‡Professor and Director, Vehicle Systems & Control Laboratory, Department of Aerospace Engineering, Associate Fellow AIAA, valasek@tamu.edu

GPS Global Positioning System
IMU Inertial Measurement Unit
MSE Mean squared error
OKID Observer/Kalman Filter Identification
TIC Theil information coefficient
UAV Unmanned aerial vehicle
VSCL Vehicle Systems + Controls Laboratory

I. Introduction

System identification of fixed-wing aircraft from flight data remains a reliable method for obtaining accurate dynamic models. The increasing availability of computational fluid dynamics software improves the accuracy of models that can be obtained in lieu of flight test results. However, using this software may be time consuming or expensive, unnecessarily so if there is ready access to the physical vehicle. The increasing prevalence of lightweight UAVs means that the topic of fixed-wing aircraft system identification has remained a focus for study in recent research. Valasek and Chen[1] consider Observer/Kalman Filter Identification (OKID) for online system identification of UAVs, and present results using nonlinear simulation. Morelli[2] summarizes historical and recent aircraft dynamic identification research at NASA Langley Research Center. These results include: real-time parameter estimation using a recursive Fourier transform; multivariate orthogonal polynomial models for globalizing wind-tunnel test data; frequency-domain approach for identifying low-order equivalent system models from flight data, applied to high angle-of-attack F-18 flights and to the Tu-144 supersonic vehicle; and modelling of unsteady aerodynamics using indicial functions. Ref. 3 employs a modified sequential least-squares algorithm for online identification of a time-varying state-space model for an F/A-18 aircraft. Rohlf[4] identifies a global model of the X-31 experimental aircraft by developing aerodynamic increment tables based on flight tests to supplement an existing database. Ref. 5 uses Hopfield Neural Networks to develop linear models by minimizing an error function. In Ref. 6, nonlinear aircraft models are identified using Global-Local Mapping Algorithm, and compares against linear models identified using OKID. More recently, Dorobantu et. al[7] perform frequency domain identification using the CIFER software package to fit a first-principles linear model.

This paper extends the previous simulation based work of Valasek and Chen[1] by using the Observer/Kalman Filter Identification (OKID) methodology to identify linear dynamic models of a UAV from flight data. While that work demonstrated that the methodology is suitable for simulation-based identification with simulated turbulence and sensor noise, the present work addresses identification from flight data acquired with actual sensors. The paper is organized as follows. Section II introduces the OKID algorithm, and Section III contains the vehicle description. Section IV details the instrumentation and measurements and Section V discusses the flight testing. Section VI presents the flight test results and describes the model identification process and selection of models, and Section VII presents conclusions.

II. Observer/Kalman Filter Identification (OKID)

OKID is developed from the eigensystem realization algorithm (ERA) for linear system identification.[8] In this section, the theoretical backgrounds of the ERA and OKID algorithms are presented. In both cases, linear discrete-time systems for the plant behavior are assumed, and have the following form:

$$\begin{aligned} \mathbf{x}_{k+1} &= A\mathbf{x}_k + B\mathbf{u}_k \\ \mathbf{y}_k &= C\mathbf{x}_k + D\mathbf{u}_k \end{aligned} \tag{1}$$

In Eq. (1), the k index in $\mathbf{x}_k$ is shorthand for $\mathbf{x}(kT)$, where T is the system sample rate and k is an integer. $\mathbf{x} \in \mathbb{R}^n$, $\mathbf{u} \in \mathbb{R}^m$, $A \in \mathbb{R}^{nxn}$, $B \in \mathbb{R}^{nxm}$, $C \in \mathbb{R}^{qxn}$, and $D \in \mathbb{R}^{qxm}$. The generic problem of system identification is to determine matrices $[A, B, C, D]$ such that a measured output sequence for $\mathbf{y}_k$ is

reproduced.

II.A. Eigensystem realization algorithm

The development here follows Refs. 9 and 10. For a discrete-time linear system of the form of Eq. (1) with zero initial conditions for $\mathbf{x}(0)$, the output sequence for the linear dynamic system is as follows:

$$\begin{aligned}
\mathbf{y}_0 &= C\mathbf{x}_0 + D\mathbf{u}_0 = D\mathbf{u}_0 \\
\mathbf{x}_1 &= A\mathbf{x}_0 + B\mathbf{u}_0 = B\mathbf{u}_0 \\
\mathbf{y}_1 &= CB\mathbf{u}_0 + D\mathbf{u}_1 \\
\mathbf{x}_2 &= A\mathbf{x}_1 + B\mathbf{u}_1 = AB\mathbf{u}_0 + B\mathbf{u}_1 \\
\mathbf{y}_2 &= C(AB\mathbf{u}_0 + B\mathbf{u}_1) + D\mathbf{u}_2 \\
&\dots \\
\mathbf{x}_{k+1} &= \sum_{i=0}^{k} A^{k-i}B\mathbf{u}_i \\
\mathbf{y}_k &= C\sum_{i=0}^{k-1}\left(A^{k-i-1}B\mathbf{u}_i\right) + D\mathbf{u}_k
\end{aligned} \tag{2}$$

Define the system Markov parameters $Y(k)$ by

$$Y(k) = \begin{cases} D & : k = 0 \\ CA^{k-1}B & : k > 0 \end{cases} \tag{3}$$

The output sequence can be written as in Eq. (4):

$$\mathbf{y}_k = \sum_{i=1}^{k} Y(k-i)\mathbf{u}_i \tag{4}$$

The ERA assumes measurements of the Markov parameters are available. They may be obtained directly by measuring the system response to a unit impulse on each of the m input channels, or indirectly as in OKID. In the former case, the jth column of $Y(k)$ is the system response $\mathbf{y}_k$ to a unit pulse on input j at $t = 0$.

The basic ERA solution procedure for obtaining a realization is as follows:

1. Construct the $r \times s$ block Hankel matrix, defined as:

$$H_{k-1} = \begin{bmatrix} Y(k) & Y(k+1) & \dots & Y(k+s-1) \\ Y(k+1) & Y(k+2) & \dots & Y(k+s) \\ \vdots & \vdots & & \vdots \\ Y(k+r-1) & Y(k+r) & \dots & Y(k+r+s-2) \end{bmatrix} \tag{5}$$

2. Compute the singular value decomposition (SVD) of $H(0)$, defined as $H(0) = R_n \Sigma S_n$.

3. The system order is determined from the relative magnitude of the singular values of $H(0)$. In theory, the system order is the number of nonzero singular values; in practice, measurement noise and machine errors will produce small singular values that should be neglected.

4. A minimum-order system realization can be written in terms of the SVD:

$$\begin{aligned}\hat{A} &= \Sigma_n^{-1/2} R_n^T H(1) S_n \Sigma_n^{-1/2} \\ \hat{B} &= \Sigma_n^{1/2} S_n^T E_r \\ \hat{C} &= E_m^T R_n \Sigma_n^{1/2} \\ \hat{D} &= Y(0)\end{aligned} \tag{6}$$

5. Modal damping and frequencies may then be obtained from the realized state matrix

II.B. Observer/Kalman Filter Identification

OKID extends the ERA to systems with nonzero initial conditions and arbitrary input sequences. Fundamentally, OKID obtains a close approximation to the Hankel matrix of Eq. 5, then follows the ERA solution procedure. The development in this section follows Refs. 8 and 1. In addition to the requirement of zero initial conditions and pulse inputs, the ERA may suffer from long computational times for lightly damped systems. OKID overcomes this issue by augmenting the discrete-time system of Eq. (1) with an observer G, as in:

$$\begin{aligned}\mathbf{x}_{k+1} = (A+GC)\mathbf{x}_k + (B+GD)\mathbf{u}_k - G\mathbf{y}_k &= \bar{A}\mathbf{x}_k + \bar{B}\mathbf{v}_k \\ \mathbf{v}_k &= \begin{bmatrix}\mathbf{u}_k \\ \mathbf{y}_k\end{bmatrix} \\ \mathbf{y}_k &= C\mathbf{x}_k + D\mathbf{u}_k\end{aligned} \tag{7}$$

The problem formulation is otherwise the same; however, the presence of nonzero initial conditions and arbitrary control inputs modifies the output sequence from Eq. (4):

$$\begin{aligned}\mathbf{x}_{k+1} &= A^{k+1}\mathbf{x}_0 + \sum_{i=0}^{k} A^{k-i} B\mathbf{u}_i \\ \mathbf{y}_k &= C\left(A^k\mathbf{x}_0 + \sum_{i=0}^{k-1}\left(A^{k-i-1}B\mathbf{u}_i\right)\right) + D\mathbf{u}_k\end{aligned} \tag{8}$$

The output sequence can be written compactly as

$$\begin{aligned}\bar{y} &= C\bar{A}^p\bar{x} + \bar{Y}\bar{V} \\ \bar{y} &\equiv \begin{bmatrix}\mathbf{y}_p & \mathbf{y}_{p+1} & \cdots & \mathbf{y}_{l-1}\end{bmatrix} \\ \bar{Y} &\equiv \begin{bmatrix}D & C\bar{B} & C\bar{A}\bar{B} & \ldots & C\bar{A}^{p-1}\bar{B}\end{bmatrix}\end{aligned} \tag{9}$$

In Eq. (9), the terms D, $C\bar{B}$, $C\bar{B}\bar{A}$, etc. are the *observer* Markov parameters. They are equivalent to Eq. (3) for the system modified by the observer G. The matrix $\bar{V}$ is the Hankel matrix composed of the augmented system inputs:

$$\bar{V} = \begin{bmatrix}\mathbf{u}_p & \mathbf{u}_{p+1} & \cdots & \mathbf{u}_{l-1} \\ \mathbf{v}_{p-1} & \mathbf{v}_p & \cdots & \mathbf{v}_{l-2} \\ \mathbf{v}_{p-2} & \mathbf{v}_{p-1} & \cdots & \mathbf{v}_{l-3} \\ \ddots & \vdots & \ldots & \vdots \\ \mathbf{v}_0 & \mathbf{v}_1 & \cdots & \mathbf{v}_{l-p-1}\end{bmatrix} \tag{10}$$

A key assumption is that $\bar{A}^p$ becomes negligibly small for some $p > 0$. Under this assumption, Eq. (9) can be written as

$$\bar{y} = \bar{Y}\bar{V} \tag{11}$$

Eq. (11) is solved for the unknown $\bar{Y}$ in a least-squares sense:

$$\begin{aligned} \bar{Y} &= \bar{y}\bar{V}^{+} \\ \bar{V}^{+} &\equiv \bar{V}^{T}(\bar{V}\bar{V}^{T})^{-1} \end{aligned} \tag{12}$$

With the solution for $\bar{Y}$, it is straightforward to partition it into the observer Markov parameters:

$$\bar{Y} = \begin{bmatrix} D & C\bar{B} & C\bar{A}\bar{B} & \dots & C\bar{A}^{p-1}\bar{B} \end{bmatrix} \equiv \begin{bmatrix} \bar{Y}_0 & \bar{Y}_1 & \bar{Y}_2 & \dots \bar{Y}_p \end{bmatrix} \tag{13}$$

For $k > 0$, the observer Markov parameters may be partitioned as:

$$\begin{bmatrix} \bar{Y}_k^{(1)} & -\bar{Y}_k^{(2)} \end{bmatrix} \equiv \begin{bmatrix} C(A+GC)^{k-1}(B+GD) & -C(A+GC)^{k-1}G \end{bmatrix}, \quad k = 1, 2, 3, \dots \tag{14}$$

Note that only the observer Markov parameters have been determined, not the system Markov parameters as required for the ERA. The system Markov parameters Y_j can be shown to be recursively related to the observer Markov parameters $\bar{Y}_j$:[1]

$$\begin{aligned} Y_j &= \bar{Y}_j^{(1)} + \sum_{i=1}^{j} \bar{Y}_i^{(2)} Y_{j-1}, \ j = 1, \dots, p \\ Y_j &= \sum_{i=1}^{j} \bar{Y}_i^{(2)} Y_{j-1}, \ j = p+1, \dots, \infty \\ D &= Y_0 = \bar{Y}_0 \end{aligned} \tag{15}$$

This determines the system Markov parameters. From the Markov parameters, ERA beginning at Eq. (5), or an equivalent algorithm, is used to realize A, B, C as before.

III. Vehicle description

The Pegasus unmanned aerial vehicle (UAV) was designed and built by the Vehicle Systems & Control Laboratory (VSCL) at Texas A&M University as a sensor and control testbed. Pegasus is configured as a high-wing, twin-boom tail aircraft designed for stability for airborne remote sensing applications. Pegasus is configured with multiple redundant, independently-actuated control effectors including eight ailerons, two elevators, and two rudders, making this vehicle ideal for experimentally simulating actuator failure or losses of control effectiveness due to damage. The tail and nose are equipped with ballast mounts, and the wings and main gear longitudinal locations are adjustable in one inch (6% of chord) increments to allow extreme flexibility in payload configuration and static longitudinal stability requirements. Pegasus is modular and can be disassembled and stored in a case measuring roughly 7 x 3 x 2 ft (l x w x h) for ease of transport. The wings and tail are constructed of fiberglass/epoxy composite over a foam core with a circular carbon fiber spar. The fuselage is constructed of aluminum and fiberglass/epoxy with foam core. The Pegasus fuselage is sized to fit a standard ATX motherboard, so there is substantial payload capacity and volume to support relatively extensive computing hardware, compared to commonly available academic research platforms.

The design gross payload is 20 lbf in the Pegasus Modular Payload Unit, a shock-mounted EIA-310 compatible rack with the following characteristics:

- Up to 6U of 19 inch chassis mounted in face-up or down orientation or
- Up to 10U of 9 inch half-rack chassis mounted in face-up or down orientation or
- Up to 6U of 9 inch half-rack chassis mounted in face-forward or back orientation or

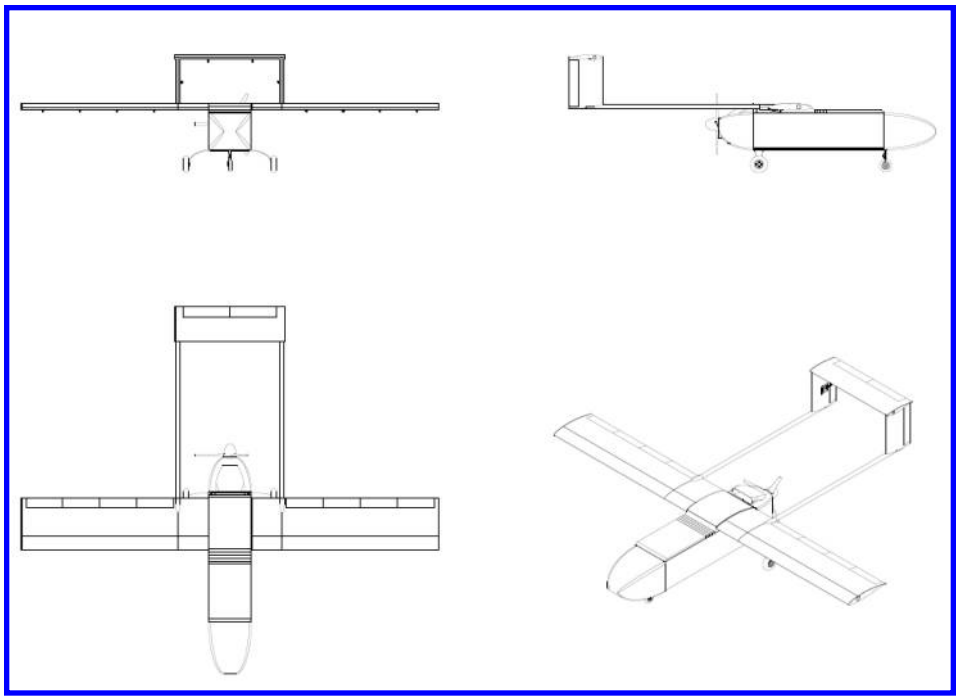

Figure 1. Pegasus external physical characteristics

- Some combination of the above.
- 12 inch flange-to-flange depth in face-up orientation
- 19.5 inch flange-to-flange depth in face-forward orientation Nose mounts are also available for up to 5 lbf of payload.

Since the first flight in February of 2012, the vehicle has approximately 15 flight hours and more than 70 flights.

IV. Instrumentation and Measurements

The vehicle is equipped with an Ardupilot Mega version 1 (APM1) autopilot. This autopilot records basic accelerometer, gyroscope, and barometric altitude measurements at 50 Hz. For system identification, this autopilot is augmented with an Aeroprobe 5-hole probe and ADC that measures airspeed, angle-of-attack, and sideslip angle. The range of recordable airspeeds is 8 - 45 m/s with a minimum airspeed resolution of 0.25 m/s. The range of values for both angle-of-attack and sideslip angle is $\pm 20^\circ$ with a flow angle resolution of 0.1°.[11] The ADC is capable of recording these values at 100 Hz either onboard via a microSD card or through serial communication to the autopilot. A rapid prototyped mount and bracket were designed to fix the 5-hole probe to the wing tip (Figure 2. Placing the ADC in the wing tip minimized the length of the tubing between the two components as well as maintained ease of assembly and disassembly of the Pegasus vehicle. Power wires run through the wing into the fuselage where the flight battery is located. The probe is fully constrained and mounted perpendicular to the leading edge of the wing as well, parallel to the chord line (Figure 3).

The APM1 samples the associated pressure transducers at 50 Hz. Additionally, global positioning system (GPS) inertial position measurements are recorded at 5 Hz.

Figure 2. Internal installation of 5-hole air data probe and air data computer

Figure 3. Wingtip installation of 5-hole airdata probe

Parameter	Value
Design payload	20 lbf
Design max t/o weight	55 lbf
Design empty dry weight	33 lb
Wing span	12 feet
Wing area	18 ft^2
Wing aspect ratio	8
Wing airfoil	NASA LS(1)-0413
Tail airfoil	NASA LS(1)-0013
Vertical tail area	3 square feet
Vertical tail aspect ratio	1.5
Horizontal tail area	3 square feet
Horizontal tail aspect ratio	3
Design wing loading	3 psf
Design power loading	6.1 lbf/hp
Design max endurance	1 hour
Design stall speed (flaps up)	26 knots
Powerplant	3W 85cc single-cylinder two-stroke reciprocating engine
Fuel capacity	1.9 lb (1.5 L)
Propeller	24 inch 3-blade carbon fiber

Table 1. Pegasus physical characteristics

Measurement	Units	Sample rate (Hz)
Inertial position	degrees latitude/longitude meters altitude	5
Three-axis acceleration	m/s^2	50
Three-axis angular velocity	rad/s	50
Barometric altitude	meters	50
Three-axis attitude estimates	radians	50

Table 2. Measured states, units, and sample rates for Pegasus system identification.

IV.A. Data processing

Angular rates and aerodynamic angles are prefiltered using Butterworth filters in MATLAB^{TM} to reduce measurement noise.[12] Initial flight tests in 2013 demonstrate problems with the aerodynamic data acquisition and autopilot attitude determination. The attitude output from the autopilot appears to approach non-zero steady-state values after excitation, which is inconsistent with the observed behavior during flight. This is interpreted as a possible effect of gyroscope bias, or simply poor accuracy in attitude estimation. In addition, for two of three flight days, performance of the air data probe is inconsistent. Angle-of-attack and sideslip angle measurements are not usable on these days, and on one of those days airspeed readings are also unusable. The process used to address these issues is described in this section.

IV.A.1. Attitude estimation

To obtain the Euler angle position history, an extended Kalman filter (EKF) is implemented based on the method outlined in Ref. 13. This filter is used to process all subsequent data and provide three-axis attitude

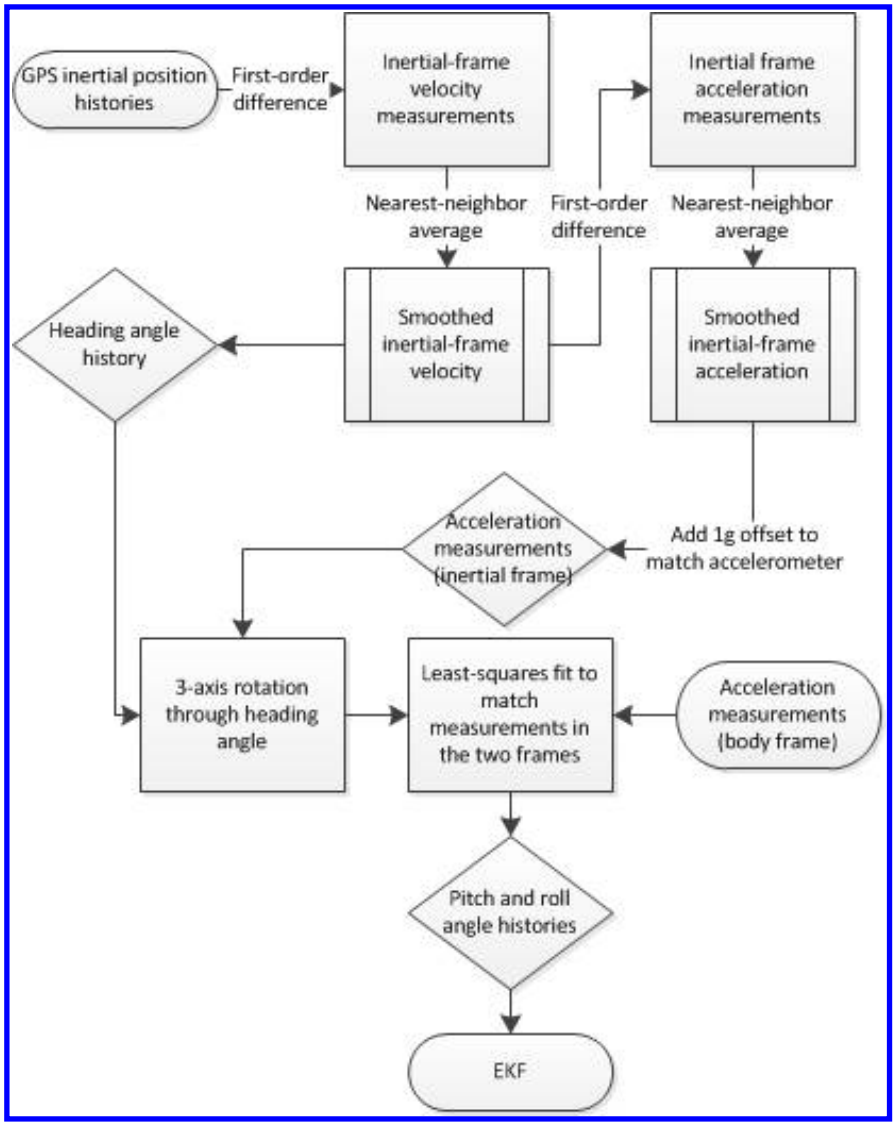

Figure 4. Flowchart of attitude estimation from GPS time histories.

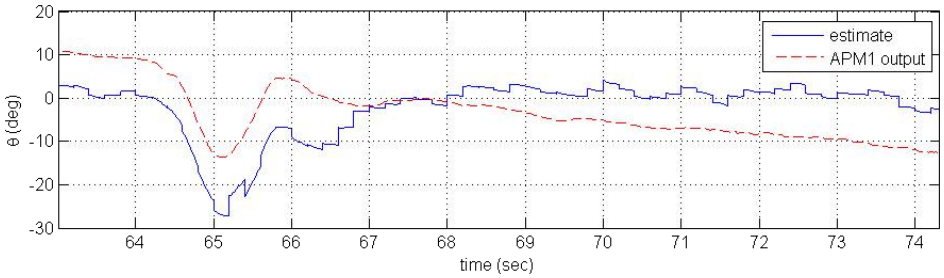

Figure 5. Comparison of pitch attitude estimates from flight data and from the EKF for one longitudinal-axis maneuver.

and gyro bias estimates. The following procedure is used, and is also summarized in the flowchart of Fig. 4:

1. GPS-derived inertial position histories are differentiated once to estimate inertial velocity in three axes.
2. To reduce noise, a two-term moving average of inertial velocity is taken and used subsequently.
3. In a north-east-down inertial coordinate system, aircraft heading is estimated from $\psi = \arctan \frac{V_{east}}{V_{north}}$.
4. Velocity histories are differentiated to produce acceleration histories, and a two-term moving average is again taken to reduce noise.
5. A value of $-g\hat{\mathbf{n}}_3$ is added to the inertial acceleration histories for consistency with accelerometer measurements, in which n^+ is the inertial coordinate system.
6. The inertial acceleration vector is transformed from the inertial frame through a three-axis rotation through ψ into an intermediate reference labeled i^+.
7. The transformed acceleration histories are now related to the aircraft body frame by a 2-axis rotation through θ and a 1-axis rotation through ϕ. In theory this vector should match the accelerometer measurements after rotating through the two still-unknown angles.
8. ϕ and θ are estimated in a least-squares sense by solving the following linearized transformation equation relating the intermediate frame i^+ to the body frame b^+:

$$\begin{bmatrix} a_1 \\ a_2 \\ a_3 \end{bmatrix}_b = \begin{bmatrix} 1 & 0 & -\theta \\ 0 & 1 & \phi \\ \theta & -\phi & 1 \end{bmatrix} \begin{bmatrix} a_1 \\ a_2 \\ a_3 \end{bmatrix}_i \tag{16}$$

9. The resulting ϕ and θ histories are treated as measurement updates in a continuous-discrete EKF.

Attitude and gyro bias estimation is a familiar estimation problem with many existing solutions. The EKF attitude estimator in Ref. 14 is modified to use the Euler angles directly instead of the quaternion to parameterize attitude, simplifying the filter by eliminating the need to enforce quaternion normality. A sample of the autopilot and EKF estimates is shown in Fig. 5.

IV.A.2. Aerodynamic angle estimation

The air data measurements are not usable from some flight days. The GPS-derived inertial velocity history and attitude estimates are used to approximate airspeed and aerodynamic angles as necessary. Body-frame velocity components U, V, W are computed by transforming the inertial frame velocity vector. The aerodynamic angles, with the assumption that the external wind is small relative to the magnitude of the aircraft velocity, are given from:

Figure 6. Pegasus in flight

$$\tan\alpha = \frac{W}{U}$$
$$\tan\beta = \frac{V}{U} \tag{17}$$

Airspeed measurements are judged to be usable from two of three flight days by comparing them to the body 1-axis inertial speed, but all of the aerodynamic data were unusable from the final day of testing. Direct airspeed measurements are found to generally yield better models, and are used whenever available. Since aerodynamic angles are usable on only one flight day, the approximation from inertial velocities described above was used on all flights for consistency in comparing model fits on different flight days. The choice of measured or estimated aerodynamic angles did not appear to significantly affect model accuracy.

V. Flight testing

Initial system identification flight tests of the Pegasus aircraft were conducted under manual control between September and November 2013. A summary of flights is given in Table 7. Longitudinal-axis maneuvers consist of an elevator doublet followed by a throttle doublet. Lateral/directional maneuvers consist of a rudder doublet followed by an aileron doublet. A total of fifteen longitudinal axis trials and thirty-two lateral/directional axis trials are conducted over three flight days.

VI. Model realization and selection

For model realization, the vehicle is assumed to be trimmed about a steady-state value, and a linear model is fit to perturbations in the aircraft states. It is assumed that vehicle bank angle ϕ is zero; this allows the aircraft linear dynamics to be decoupled into independent longitudinal and lateral/directional axes, each with two controls. All angular rates are assumed to be constant in the steady state. The longitudinal axis variables are perturbed airspeed, angle-of-attack, pitch rate, and pitch angle, with elevator and throttle as controls. For the lateral/directional axis, the perturbed variables are sideslip angle, roll rate, yaw rate, and roll angle, with aileron and rudder controls.

To identify models from the processed flight data, the data are manually segmented into each longitudinal

or lateral/directional maneuver. A model is then fitted to each data segment. For validation, control inputs are fed back into the identified model, starting at the measured initial state, and the measured and predicted responses are compared.

Models are verified against both the data used in identification and time histories from other segments. Both mean squared error (MSE) and the Theil inequality coefficient (TIC) are used as metrics of fit. MSE is defined in terms of the measured output $\tilde{y}_k$ and predicted output $\hat{y}_k$ as in Eq. (18):

$$MSE = \frac{\sum_{k=1}^{N}(\tilde{y}_k - \hat{y}_k)^2}{N} \tag{18}$$

The TIC is defined as follows:

$$TIC = \frac{\sqrt{1/N\sum_{k=1}^{N}(\tilde{y}_k - \hat{y}_k)^2}}{\sqrt{1/N\sum_{k=1}^{N}\tilde{y}_k^2} + \sqrt{1/N\sum_{k=1}^{N}\hat{y}_k^2}} \tag{19}$$

Eq. (19) yields a vector whose members are between 0 and 1, and can be evaluated across one data set or several. $TIC = 0$ implies the predictions match the data exactly and $TIC = 1$ implies maximum inequality. Acceptable values vary, but a range of $0.25 < TIC < 0.3$ is considered to indicate good agreement.[15]

Models are first downselected by considering MSE, and models with relatively high MSE are removed. If multiple models with similar qualitative behavior remain, TIC is used to further identify goodness-of-fit. The identified models for the two axes are given in the appendix.

VI.A. Longitudinal model selection

Models are evaluated by computing the mean squared error in predicting the data in all other segments on the same day. The models on each day with consistently good performance are further downselected by comparison against data from other days. Figs. 7-8 plot the base 10 logarithm of the mean squared error for each model evaluated in this fashion. For each trial and state, the total MSE across all data on a given flight day is plotted. Smaller values indicate a more accurate fit.

Based on the preceding analysis, three models were evaluated in terms of MSE against data from other flight days: Models 1 and 3 from day 1 and Model 2 from day 2. Table 3 collects the MSEs for all flight days when these models are evaluated in this fashion. Based on these results, either Day 1 Trial 3 or Day 2 Trial 2 have good performance that is relatively consistent across data sets.

Model	$log_{10}(MSE_u)$	$log_{10}(MSE_\alpha)$	$log_{10}(MSE_q)$	$log_{10}(MSE_\theta)$
Day 1 Trial 3	1.237	-1.791	-1.446	-1.364
Day 1 Trial 3	1.625	-2.082	-0.886	-0.938
Day 1 Trial 1	1.909	-1.394	-1.582	-1.305
Day 1 Trial 1	2.338	-0.355	-1.236	-0.887
Day 2 Trial 2	1.899	-0.701	-1.736	-0.838
Day 2 Trial 2	1.126	-1.720	-2.253	-1.834

Table 3. Mean squared errors of the best Pegasus longitudinal models identified using OKID.

To further compare the two models, the Theil inequality coefficient (TIC) is computed. The TIC is computed for the final two models over a set of five trials that have similar initial conditions. Two trials are from day 1 and three from day 3. Model accuracy in terms of TIC is quite similar between the two models, which indicates a certain level of consistency in the identification process. Ultimately, the Day 3 Trial 2 model is preferred because of its good accuracy in replicating u and α.

Comparisons of measured outputs with those predicted by the identified model are shown in Fig. 9 for two flight maneuvers. The model shows good agreement with predicted airspeed and angle-of-attack relative to other models, and this is a primary reason for its selection.

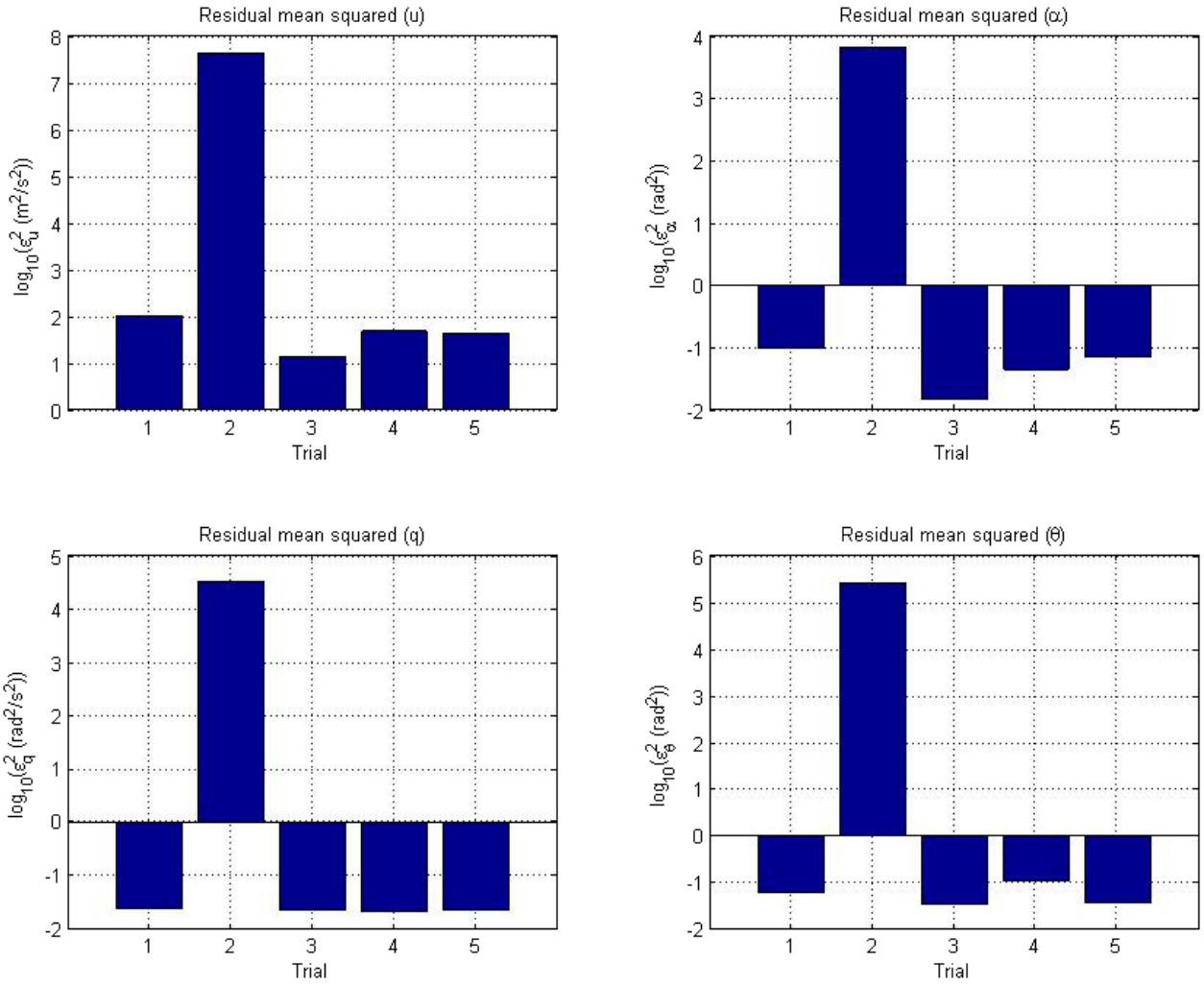

Figure 7. Pegasus longitudinal-axis MSEs for day 1 of Pegasus flights.

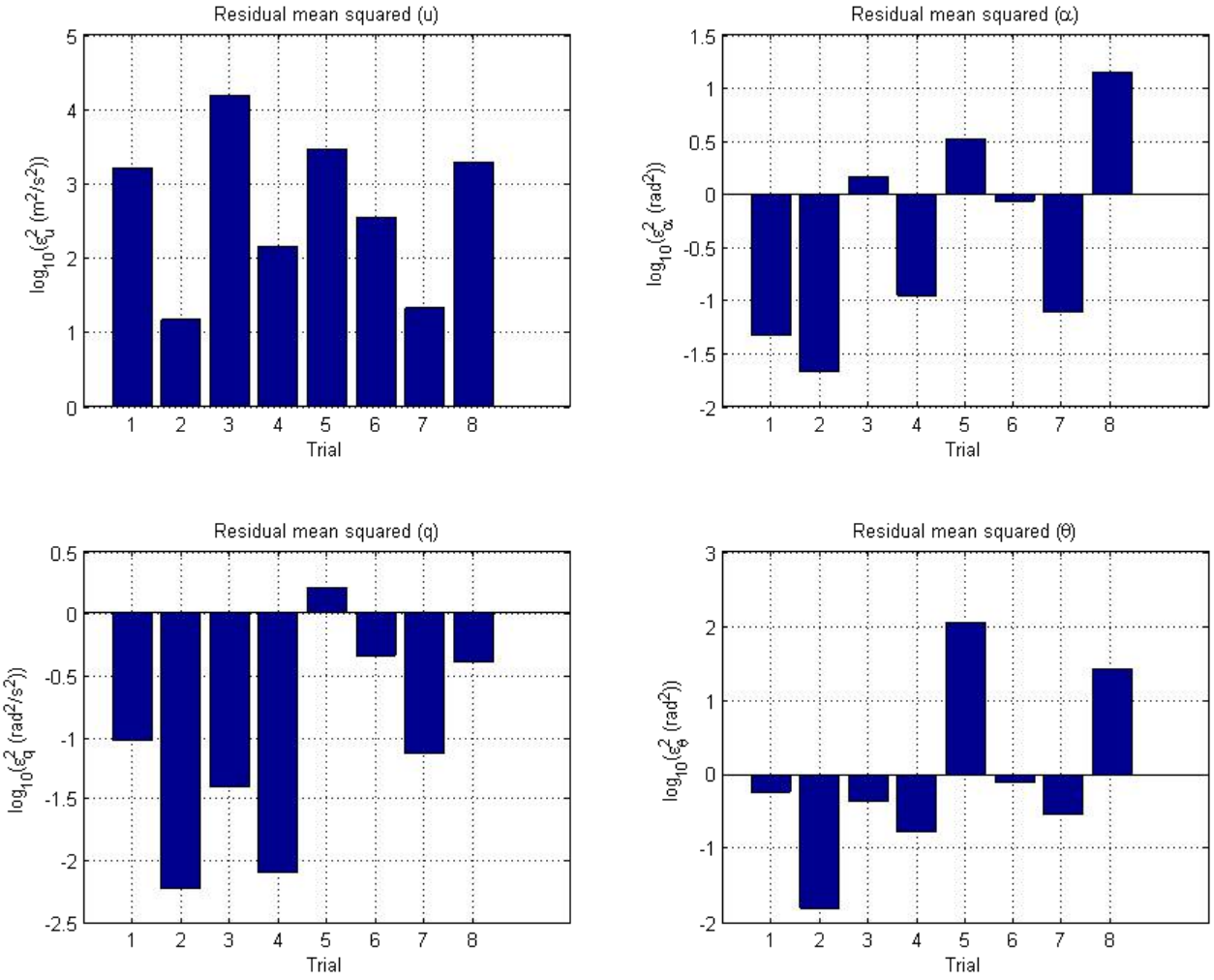

Figure 8. Pegasus longitudinal-axis MSEs for day 2 of Pegasus flights.

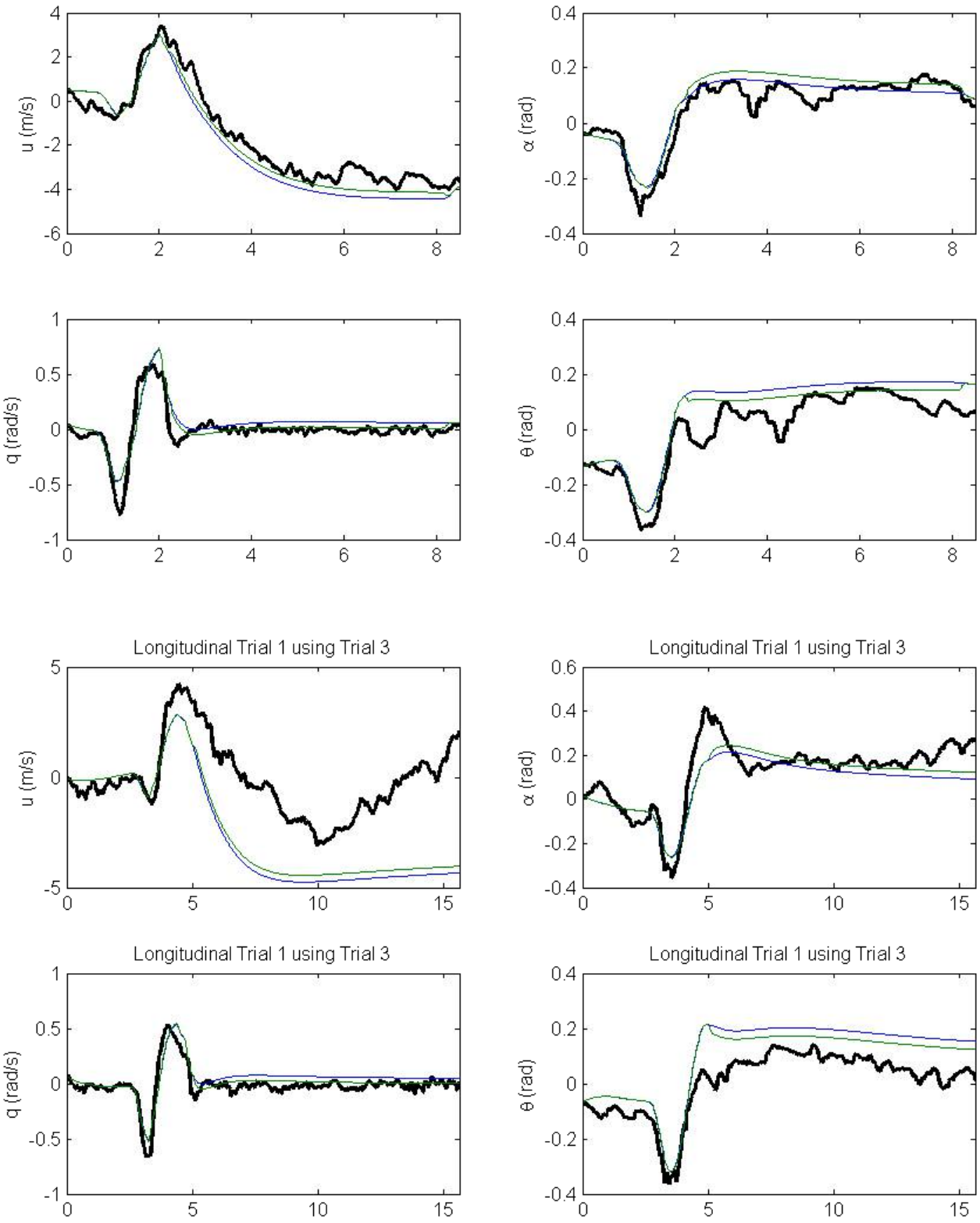

Figure 9. Comparison of longitudinal axis time histories and Pegasus model predicted outputs. Flight data are indicated by the thick black lines.

Day 1 Trial 3

Trial	TIC_u	TIC_α	TIC_q	TIC_θ
Day 1 Trial 1	0.8607	0.2410	0.3922	0.4303
Day 1 Trial 3	0.4673	0.2093	0.2906	0.4096
Day 2 Trial 2	0.8514	0.3459	0.3812	0.5575
Day 2 Trial 3	0.9214	0.2766	0.4391	0.7971
Day 2 Trial 4	0.7214	0.3326	0.3618	0.4647
Total	0.7252	0.4445	0.5527	0.7020

Day 2 Trial 2

Trial	TIC_u	TIC_α	TIC_q	TIC_θ
Day 1 Trial 1	0.9103	0.5004	0.2863	0.4010
Day 1 Trial 3	0.4866	0.3521	0.2468	0.1611
Day 2 Trial 2	0.4364	0.2213	0.2975	0.4519
Day 2 Trial 3	0.8749	0.2630	0.2606	0.09451
Day 2 Trial 4	0.6627	0.3706	0.2766	0.5007
Total	0.7482	0.5109	0.3841	0.5359

Table 4. Comparison of Theil inequality coefficient for two Pegasus longitudinal models with best performance in terms of mean squared error.

Trial	TIC_β	TIC_p	TIC_r	TIC_ϕ
Day 1 Trial 2	0.2514	0.0985	0.2415	0.2810
Day 1 Trial 5	0.4720	0.1081	0.3888	0.2144
Day 1 Trial 7	0.4008	0.1332	0.4671	0.2874
Day 1 Trial 10	0.4209	0.1232	0.3814	0.4454
Day 1 Trial 12	0.4869	0.1310	0.3965	0.3308
Day 1 Trial 14	0.4719	0.0837	0.2043	0.4052
Day 2 Trial 2	0.3332	0.1303	0.2752	0.6342
Day 2 Trial 11	0.5627	0.2805	0.4801	0.4012
Day 2 Trial 13	0.5117	0.1942	0.4290	0.3904
Day 2 Trial 15	0.3557	0.1529	0.2733	0.3111
Day 2 Trial 17	0.6151	0.2232	0.5628	0.1623

Table 5. TIC for Pegasus lateral/directional models with steady-state bank angle less than 5°. Each TIC value is computed by evaluating the model against the data used to generate it.

VI.B. Lateral/directional model selection

One model is fit to each of the thirty-two lateral/directional trials from two days of flying. In some flight segments, the pilot gave multiple doublet commands consecutively; each individual doublet is treated as a trial, and so is the string of consecutive doublets. This means that some data are repeated among the trials. In selecting the best models, one important consideration is the bank angle at the beginning of the maneuver. The decoupling of aircraft longitudinal and lateral/directional axis dynamics is only possible for a steady-state bank angle of zero. Therefore, only trials for which the initial bank angle has magnitude less than 5° are considered. This effectively eliminates twenty-two models. MSE is found not to differ greatly among the remaining models, so each model is evaluated in terms of the TIC against the data used to generate the model. These TIC values are tabulated in Table 5.

Trial	TIC_β	TIC_p	TIC_r	TIC_ϕ
Day 1 Trial 2	0.4799	0.1437	0.2646	0.5310
Day 2 Trial 3	0.5168	0.1698	0.3934	0.5124
Day 2 Trial 15	0.6033	0.3323	0.4616	0.8200

Table 6. Total TIC for three candidate Pegasus lateral/directional models evaluated across all the sets of data considered in Table 5.

Based on Table 5, three models are selected for further evaluation: Day 1 Trial 2, Day 2 Trial 2, and Day 3 Trial 15. The TIC of these three models is then computed for every test in the set of trials in Table 5. These results are given in Table 6. For brevity, only the total TIC computed across all eleven data sets is shown for the three candidate models. From these results, it is clear that the model from Day 1 Trial 2 has the lowest TIC for three of the four states. This model also shows reasonably good model fitting qualitatively (see Fig. 10), so it is selected as the linear lateral/directional model for the Pegasus system.

Fig. 10 shows a comparison of measured outputs and model-predicted outputs for two lateral/directional trials. The identified model shows reasonably good tracking of the measured states even when compared against the longer trials in the data set, indicating good agreement between the measurements and predicted outputs.

VII. Conclusions

This paper has presented flight test results for experimental identification of an unmanned air vehicle using the Observer/Kalman Filter Identification methodology. This has included a summary of flight test dates and procedures, a description of data post-processing to correct for unreliable IMU and aerodynamic measurements, and the presentation of identified model sample fits. Comparison of model predicted outputs and measured outputs for both longitudinal and lateral/directional models indicates good consistency between the identified model and flight data. Based upon the results presented, it is concluded that the Observer/Kalman Filter Identification method is suitable for the problem of generating accurate linear system models of nonlinear, rigid-body aircraft dynamics.

In future work, this identified models will be used to synthesize flight control laws. Nonlinear model fits will also be considered for greater accuracy. Additional flight tests will be conducted with a high-fidelity inertial measurement unit to improve the current results.

Acknowledgments

This work has been supported by the National Science Foundation Graduate Research Fellowship Program. This support is gratefully acknowledged by the authors.

Appendix A: Identified linear models

Identified continuous-time longitudinal and lateral/directional models are presented for a flight speed of 102.7 feet/second at 400 feet altitude. The longitudinal model is given by Eqs. 20-24.

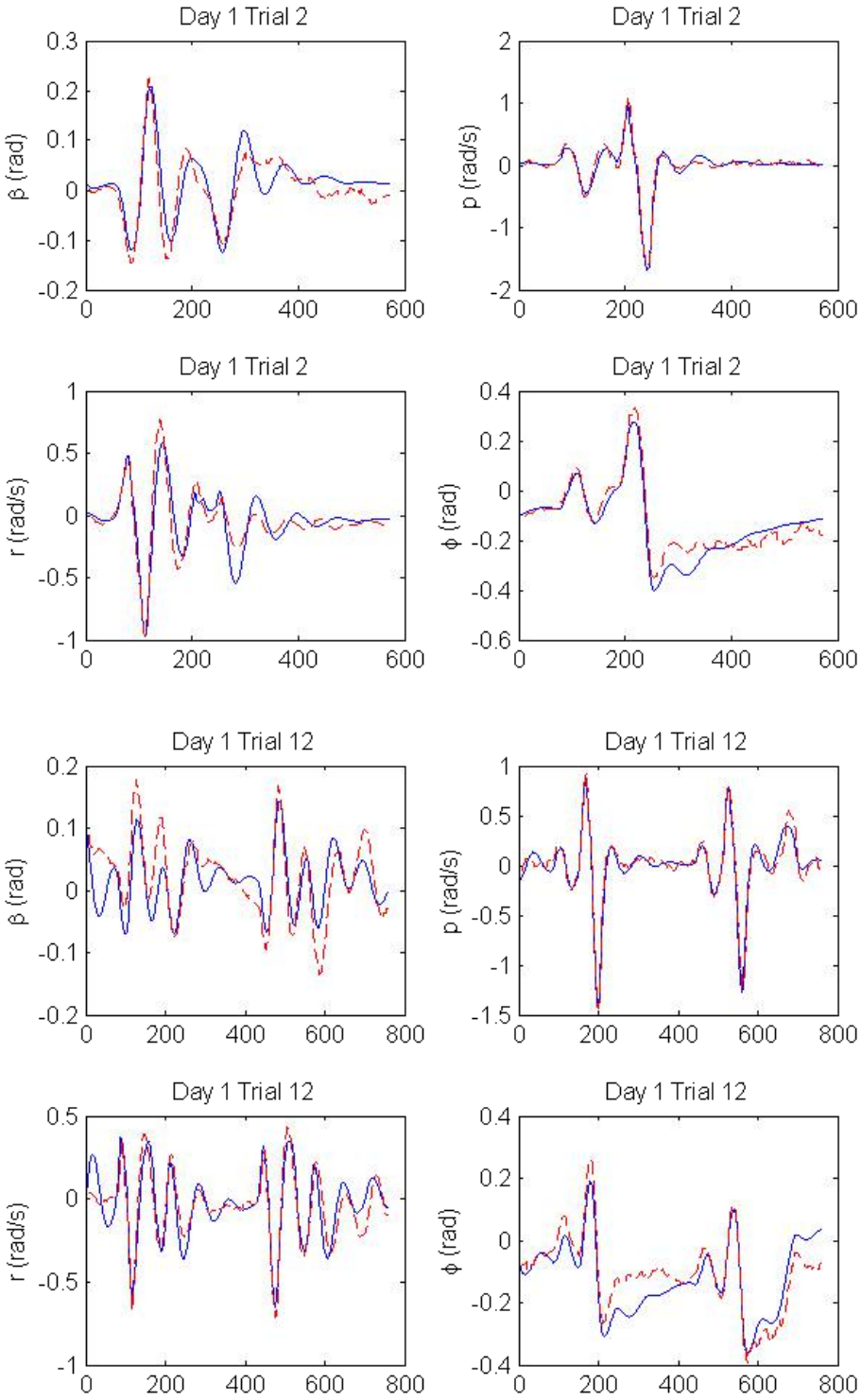

Figure 10. Sample model fitting for selected Pegasus lateral/directional model. Solid lines indicate model predicted outputs.

$$\dot{\mathbf{x}} = \begin{bmatrix} -0.796 & -6.86 & -3.199 & -0.620 \\ 0.0266 & -0.744 & 0.169 & 0.664 \\ -0.0983 & 2.466 & -4.21 & -1.64 \\ 0.000732 & 0.181 & 0.603 & -0.392 \end{bmatrix} \mathbf{x} + \begin{bmatrix} -30.2 & 3.2609 \\ -1.70 & -0.114 \\ -15.4 & 0.139 \\ -1.52 & -0.0301 \end{bmatrix} \begin{bmatrix} \delta_e \\ \delta_t \end{bmatrix} \tag{20}$$

$$\begin{bmatrix} u \\ \alpha \\ q \\ \theta \end{bmatrix} = \begin{bmatrix} 1 & 0 & 0 & 0 \\ 0 & 1 & 0 & 0 \\ 0 & 0 & 1 & 0 \\ 0 & 0 & 0 & 1 \end{bmatrix} \mathbf{x} + \begin{bmatrix} -0.125 & -0.431 \\ 0.0523 & -0.0421 \\ -0.0631 & 0.0651 \\ 0.0409 & 0.0425 \end{bmatrix} \begin{bmatrix} \delta_e \\ \delta_t \end{bmatrix} \tag{21}$$

$$U_1 = 30.3 \text{ m/s} \tag{22}$$

$$\alpha_1 = 0.0 \text{ rad} \tag{23}$$

$$\theta_1 = 0.0 \text{ rad} \tag{24}$$

The identified continuous-time lateral/directional model is given by Eqs. 25 and 26.

$$\dot{\mathbf{x}} = \begin{bmatrix} -1.56 & 0.193 & -0.948 & 0.124 \\ -11.2 & -4.79 & 1.12 & -2.77 \\ 12.2 & -2.33 & 0.0539 & 0.845 \\ -0.905 & 0.607 & 0.0131 & -0.2300 \end{bmatrix} \mathbf{x} + \begin{bmatrix} -0.116 & -0.590 \\ 112 & -3.30 \\ 32.3 & 14.1 \\ 6.79 & -0.656 \end{bmatrix} \begin{bmatrix} \delta_a \\ \delta_r \end{bmatrix} \tag{25}$$

$$\begin{bmatrix} \beta \\ p \\ r \\ \phi \end{bmatrix} = \begin{bmatrix} 1 & 0 & 0 & 0 \\ 0 & 1 & 0 & 0 \\ 0 & 0 & 1 & 0 \\ 0 & 0 & 0 & 1 \end{bmatrix} \mathbf{x} + \begin{bmatrix} 0.0461 & -0.000266 \\ -0.625 & -0.0456 \\ -0.384 & -0.249 \\ -0.0139 & -0.0144 \end{bmatrix} \begin{bmatrix} \delta_a \\ \delta_r \end{bmatrix} \tag{26}$$

Appendix B: Summary of flight tests

Date	Time	Wind (mean/max)	Objectives	Center of gravity	Weight (lbf)	Time of flight (min.sec)
2014/09/14	10:45 CDT	2/7 mph	Longitudinal	51 in	93.5	12.50
2014/11/02	18:00 CST	6/13 mph	Lateral/directional	49 in	99	8.0
2014/11/03	14:30 CST	4/12 mph	Lateral/directional	49 in	99	6.40
2014/11/03	15:00 CST	4/12 mph	Longitudinal	49 in	99	9.10

Table 7. Test matrix for Pegasus system identification flight tests. Daily average and high steady wind values, measured at a nearby weather station, are shown.[16] Center of gravity is expressed as the distance along the body 1-axis aft of the vehicle nose.

References

[1]Valasek, J. and Chen, W., "Observer/Kalman Filter Identi cation for Online System Identification of Aircraft," *Journal of Guidance, Conrol, and Dynamics*, Vol. 26, No. 2, March-April 2003, pp. 347–353.

[2]Morelli, E. A. and Klein, V., "Application of System Identification to Aircraft at NASA Langley Research Center," *Journal of Aircraft*, Vol. 42, No. 1, January-February 2005, pp. 12–25.

[3]Ward, D. G. and Monaco, J. F., "System identification for Retrot Recongurable Control of an F/A-18 Aircraft," *Journal of Aircraft*, Vol. 42, No. 1, January-February 2005, pp. 63–72.

[4]Rohlf, D., "Global Model Approach for X-31 VECTOR System Identication," *Journal of Aircraft*, Vol. 42, No. 1, January-February 2005, pp. 54–62.

[5]Hu, Z. and Balakrishnan, S., "Parameter Estimation in Nonlinear Systems Using Hopeld Neural Networks," *Journal of Aircraft*, Vol. 42, No. 1, January-February 2005, pp. 41–53.

[6]Marwaha, M., Valasek, J., and Singla, P., "GLOMAP Approach for Nonlinear System Identification of Aircraft Dynamics Using Flight Data," *Proc. AIAA Atmospheric Flight Mechanics Conference*, 2008, pp. 1–19.

[7]Andrei Dorobantu, Austin M. Murchy, B. M. and Balas, G. J., "Frequency Domain System Identification for a Small, Low-Cost, Fixed-Wing UAV," No. AIAA 2011-6719 in AIAA Guidance, Navigation, and Control Conference, August 2011.

[8]Juang, J.-N., "Applied system identification," 1994.

[9]Juang, J.-N. and Pappa, R. S., "An Eigensystem Realization Algorithm for Model Parameter Identification and Model Reduction," *Journal of Guidance, Control, and Dynamics*, Vol. 8, No. 5, 1985, pp. 620–627.

[10]Peterson, L. D., "Efficient computation of the eigensystem realization algorithm," *Journal of Guidance, Control, and Dynamics*, Vol. 18, No. 3, 1995, pp. 395–403.

[11]Aeroprobe, "Air Data system," Tech. rep., datasheet.

[12]"Butterworth filter design," `http://www.mathworks.com/help/signal/ref/butter.html`, Accessed March 31, 2014.

[13]Kingston, D. B. and Beard, R. W., "Real-time attitude and position estimation for small UAVs using low-cost sensors," *AIAA 3rd Unmanned Unlimited Technical Conference, Workshop and Exhibit*, sn, 2004, pp. 2004–6488.

[14]Crassidis, J. L. and Junkins, J. L., *Optimal estimation of dynamic systems*, CRC press, 2nd ed., 2011.

[15]Jategaonkar, R. V., *Flight vehicle system identification: a time domain methodology*, Vol. 216, American Institute of Aeronautics and Astronautics Reston, Virginia,, USA, 2006.

[16]"Personal Weather Station: KTXBRYAN19," `http://www.wunderground.com/personal-weather-station/dashboard?ID=KTXBRYAN19#history/data/s20130914/e202404/mtoday`, Accessed April 15, 2014.